Ultracompact microinterferometer-based fiber Bragg grating interrogator on a silicon chip

J. Elaskar, F. Bontempi, P. Velha, R. M. A. Ayaz, L. Tozzetti, S. Faralli, F. Di Pasquale, C. J. Oton

***Abstract*—We report an interferometer-based multiplexed fiber Bragg grating (FBG) interrogator using silicon photonic technology. The photonic-integrated system includes the grating coupler, active and passive interferometers, a 12-channel wavelength-division-multiplexing (WDM) filter, and Ge photodiodes, all integrated on a 6x8 mm^2 silicon chip. The system also includes optical and electric interfaces to a printed board, which is connected to a real-time electronic board that actively performs the phase demodulation processing using a multitone mixing (MTM) technique. The device with active demodulation, which uses thermally-based phase shifters, features a noise figure of σ = 0.13 pm at a bandwidth of 700 Hz, which corresponds to a dynamic spectral resolution of 4.9 fm/Hz$^{1/2}$. On the other hand, the passive version of the system, based on a 90º-hybrid coupler, features a noise figure of σ = 2.55 pm at a bandwidth of 10 kHz, also showing successful detection of a 42 kHz signal when setting the bandwidth to 50 kHz. These results demonstrate the advantage of integrated photonics, which allows the integration of several systems with different demodulation schemes in the same chip and guarantees easy scalability to a higher number of ports without increasing the dimensions or the cost.**

***Index Terms*— silicon photonics, optical fiber sensing, fiber Bragg grating, integrated sensor**

I. Introduction

SILICON photonics technology enables the fabrication of optical systems on the surface of a silicon chip. The main advantage of this technology is its compatibility with complementary metal-oxide-semiconductor (CMOS) platform, which allows leveraging highly developed fabrication foundries with unique precision, combined with capability for very high-scale mass production [1]. This feature makes it possible to fabricate complex optical systems at a very low cost per unit. After more than two decades of research and development, it has recently reached commercial applications mostly in the telecom sector. However, other applications such as optical sensing could greatly benefit from these advantages, enabling high performance at very low cost and power consumption. Optical fiber sensing is a technology with unique advantages with respect to electronic sensors, including among others, small size, immunity to electromagnetic interference, ease of multiplexing, and possible integration into smart materials and structures. In particular, fiber Bragg grating sensors (FBGs) [2] can be sensitive to temperature, strain, pressure, and many other physical, biochemical and environmental parameters, when used with suitable transducers, and have reached a significant market volume in various application sectors[3-5]. However, these sensors require a reading unit, called FBG interrogator, to perform the readout of several FBG reflected peaks at the same time. These units are typically bulky and expensive, which limits their market penetration. Silicon photonics can alleviate this problem with reading units characterized by smaller size, weight, cost, power consumption, and more robust to harsh environments.

There have been previous demonstrations of integrated-optic FBG interrogators. One method consists of using an arrayed waveguide grating filter for Wavelength Division Multiplexing (WDM) as a spectrometer [6]. With this method, the peak positions can be extracted using a center-of-mass estimation from the powers measured in adjacent channels. However, this method requires many more optical ports than sensing channels. Another method is to use micro-ring resonators, which are easy to integrate in silicon photonics, and are also easy to tune with integrated heaters. The wavelength can be extracted passively by tuning the ring to the FBG maximum slope, as in [7], or by actively sweeping or dithering the ring along a wider range, as in[8,9]. The main drawback of using ring resonators is the free-spectral range (FSR), which is limited to 20-30 nm, and their tunability range, which is also limited by a similar amount.

Another method to extract the wavelength consists in using an integrated interferometer. If the branches are unbalanced by a certain optical path difference, a wavelength shift of the input light generates a phase shift which is proportional to the path difference. However, extracting the phase along a wide range without responsivity fading requires keeping the interferometer in quadrature. A feedback loop can be set to actively track the peak, but this limits the interferometer to one single measuring point. Another method consists of using an interferometer with a hybrid output coupler, which generates two or three signals with different dephasing (90º or 120º) [10]. These signals can

Manuscript submitted on 3rd November 2022. This work was supported by the Italian Space Agency (ASI) through project ARTEMIDE, funded by the program "Nuove idee per la componentistica spaziale del futuro TRL" and by the Italian Ministry of University and Research through the Department of Excellence in Robotics & AI.

All authors are with Scuola Superiore Sant'Anna, Institute of Mechanical Intelligence, Via G. Moruzzi 1, 56124, Pisa, Italy. P. Velha is now at University of Trento, Dipartimento di Ingegneria e Scienza dell'Informazione, Via Sommarive 9, Povo, Trento, Italy.

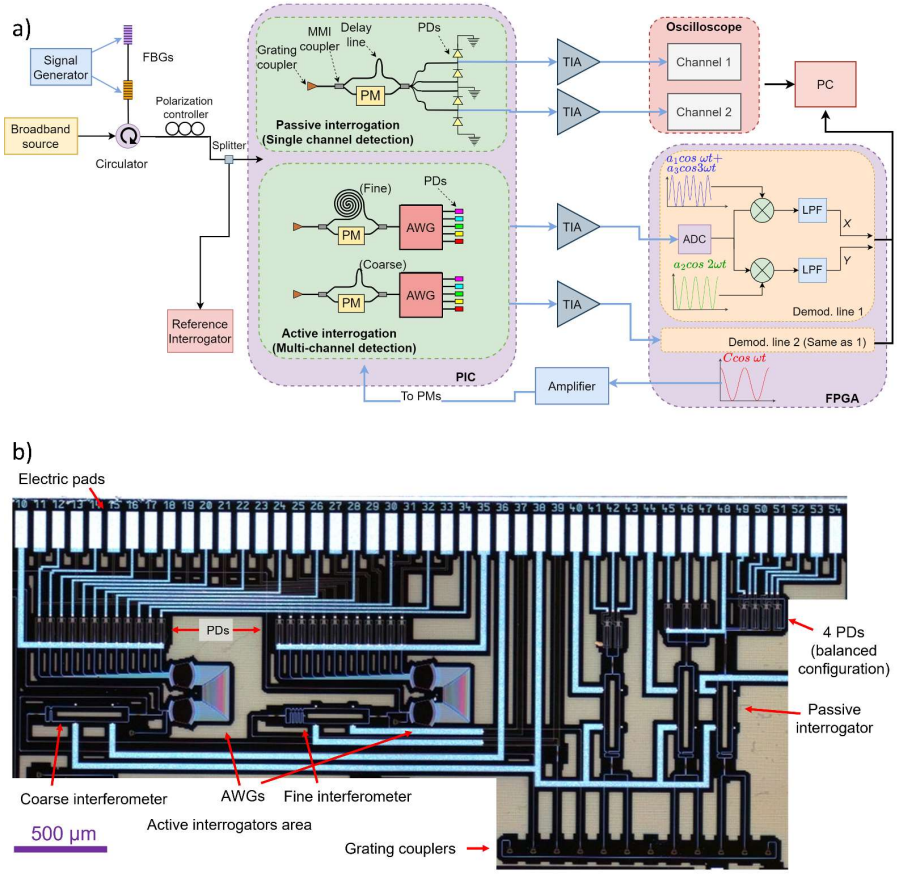

Fig. 1 (a) Schematic of the experimental system (b) Picture of the photonic chip taken with a microscope. PD: photodiode, AWG: Arrayed wavelength grating, TIA: Trans-impedance amplifier, MMI: Multimode interference, PIC: Photonic integrated circuit.PM: Phase-modulator

be used to extract the phase with no responsivity fading, although this technique requires more than one signal acquisition per sensing point. Finally, another technique called Phase Generated Carrier (PGC) consists in dithering the interferometer with a sinusoidal wave and extracting the phase from the different harmonics of the output signal [11]. This is the method used in [12],[13] for FBG interrogation.

In this paper, we report experimental results concerning a full optical system on chip (including photodiodes), which is interfaced with a printed circuit board (PCB) and with a pigtailed fiber array. The system also includes a real-time phase demodulation scheme based on multitone mixing, implemented in a Field-Programmable Gate Array (FPGA) card. We also compare the results with a passive demodulation technique using a 90º-hybrid as an output coupler.

The paper is organized as follows. In Sec. II we explain the fundamentals for wavelength detection using interferometry, and the techniques that we used to do so. In Sec. III we describe the whole system in detail. In Sec. IV we present the experimental results, first for the active interrogation with both fine and coarse interferometers, and then for the passive interrogation ones, showing the advantages and limitations of each approach. Finally, in Sec. V we draw the conclusions of the work.

II. Demodulation Technique

The main device of the integrated optical system is an unbalanced interferometer which generates a fringe pattern with a free spectral range ($\Delta\lambda_{FSR}$) equal to:

$$\Delta\lambda_{FSR} = \frac{{\lambda_0}^2}{n_g \Delta L} \quad (1)$$

where λ_0 is the central wavelength, n_g the group index of the waveguide, and ΔL the path difference. This means that when there is a wavelength shift $\Delta\lambda$ at the input, the phase change detected at the output will be equal to:

$$\Delta\phi = 2\pi \frac{\Delta\lambda}{\Delta\lambda_{FSR}} \quad (2)$$

However, to measure the phase from the light intensity at the output, the sinusoidal response generates responsivity fading when the phase moves away from the quadrature points. To avoid that, one can use a hybrid coupler at the output. If a 90º hybrid is used, the outputs would be proportional to:

$$X \propto cos(\phi) \quad (3a)$$
$$Y \propto sin(\phi) \quad (3b)$$

which allows us to extract the phase from a simple arc tangent:

$$\phi = arg(X + jY) \quad (4)$$

This technique requires at least two ports per sensing point. Alternatively, the phase can also be extracted using a 2x3 coupler at the output of the MZI, where each output signal would be:

$$I_n \propto cos\left(\phi + \frac{2\pi(n-1)}{3}\right) \text{ for } n = 1,2,3 \quad (5)$$

Then, the phase can be recovered by using:

$$X = I_2 + I_3 - 2I_1 \quad (6a)$$
$$Y = \sqrt{3}\,(I_2 - I_3) \quad (6b)$$

And then, eq. (4) is used to extract the phase. Nevertheless, there can be some deviations between the 3 outputs and their phase difference might not be exactly $2\pi/3$. To solve this problem, in [10] it is proposed a modification to eqs. (6a) and (6b) to compensate for the deviations. However, this technique requires the measurement of 3 simultaneous signals per sensing point, which complicates the system.

To simplify multiplexing, it is much more convenient to have only one signal per sensing point. This can be done by applying an active modulation signal to the interferometer. If the modulation signal is sinusoidal with an angular frequency ω, the signal output is proportional to:

$$I = A + B\,cos(C\,cos(\omega t) + \phi) \quad (7)$$

where C is the modulation depth. This technique is called Phase Generated Carrier (PGC) demodulation, and it allows the extraction of signals proportional to the cosine and the sine of the phase by mixing the signal with the first and second harmonics of the modulation frequency, and low-pass filtering [11]. In [14], we demonstrated a more robust demodulation technique which includes a third harmonic component in the mixing signal, called multitone mixing. This technique strongly reduces distortion of the phase in presence of fluctuations in the modulation depth.

To implement the method, we digitally generate two synthetic functions f_1 and f_2 defined as:

$$f_1(t) = a_1\,cos\,\omega\,t + a_3\,cos\,3\,\omega t \quad (8a)$$
$$f_2(t) = a_2\,cos\,2\,\omega t \quad (8b)$$

where the a_i coefficients are chosen to equalize the slopes of the combinations of Bessel functions [14]. For the specific modulation depth of $C = 0.84\pi$, the coefficients are $a_1 = 1$, $a_2 = 2.5806$ and $a_3 = -3.0339$.

These two functions are digitally mixed with the signal coming from the output of the interferometer, and low-pass-filtered, generating the signals X and Y:

$$X = LPF\{I \otimes f_1\} \quad (9a)$$
$$Y = LPF\{I \otimes f_2\} \quad (9b)$$

Where LPF stands for low-pass filter, and the $\otimes$ symbol stands for mixing (digital multiplication) of the signals. Once the functions X and Y are calculated, they can be used to extract the phase using Eq. 4.

III. System description

The system is depicted in Fig. 1(a). A fiber-coupled SLED source (model Denselight DL-BX9-CS5169A, with central wavelength 1550 nm, 80 nm 3dB bandwidth, and power 12 dBm) was connected to two FBGs (with central wavelengths at 1540.7 nm and FWHM 0.6 nm, and 1548.5 nm and FWHM 0.28 nm) through a circulator. Both FBGs were actuated at constant room temperature using piezoelectric transducers (PZT). The reflected light passed through a polarization controller, which was adjusted to optimize the signal for the PIC, and then the light was split into two branches, one coupled to the chip and the other one sent to the reference FBG interrogator (model Ibsen Photonics I-MON-512-USB, with a sample rate of 3kS/s).

The silicon chip is shown in Fig. 1(b). It was fabricated at AMF foundry [15] using deep-UV lithography, in a multi-project wafer (MPW) run. The technology uses silicon-on-insulator (SOI) wafers with a silicon layer thickness of 220 nm, and our design includes a 70 nm partial etch, metal heaters, and Ge photodiodes. The dimensions of the chip are 6x8 mm^2. The input light was connected to the chip through a grating coupler and then divided into two interferometers for active phase demodulation with different responsivities, which we named *fine* and *coarse*. The *fine* interferometer had a nominal FSR of 1.5 nm, while the *coarse* interferometer had a nominal FSR of 6 nm, as shown in Fig. 3 (a). The reason for including two versions is to compare them considering the trade-off between range and responsivity. Both interferometers included identical metal heaters in one branch for active phase modulation, which had a length of 200 µm, a resistance of 1.2 kΩ, a tuning efficiency of 36 mW/FSR, and a response time τ = 13.1 µs. Fig. 2 shows the heater response to a square signal along with the exponential curves used to calculate its response time.

Since the phase response is proportional to the electrical power, not to the voltage, the sinusoidal shape in phase was generated by sending a sinusoidal signal with zero offset and half of the modulation frequency, which generates a power signal with a sinusoidal shape at the nominal frequency. The amplitude of the voltage signal sent to the heater was 15.6V peak-to-peak, to generate the nominal C value of 0.84π, with a frequency of 6.2 kHz. As demonstrated in [14], slight modulation depth variations do not generate distortion in the demodulated signal when using an MTM demodulation algorithm.

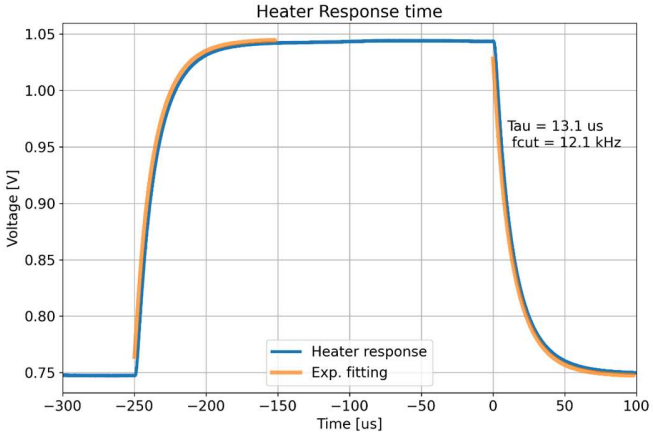

Fig. 2. Heater response signal to a square signal

As shown in Fig. 1 a), to perform active phase demodulation of FBG sensors at different wavelengths (multichannel detection), each interferometer was connected to an arrayed-waveguide grating (AWG) which was designed using Luceda IPKISS AWG designer toolbox. The fabricated AWG shown in Fig. 3 b) has 12 channels with a channel spacing of 4 nm, centered at 1550 nm. This allowed us to cover a total range of 48 nm. Finally, all the AWG outputs were sent to Germanium photodiodes, which were connected to a row of pads with a common anode configuration.

Note that the passive interrogation scheme, also shown in Fig. 1 a), has been only characterized for single channel detection at 1548 nm. Multichannel detection in this case would require the connection of each output of the 90º-hybrid coupler to a different AWG.

The chip was packaged to a PCB using wire bonding and pigtailing of a fiber array for the optical input. The chip was mounted on a Peltier module to control and stabilize its temperature using a TEC control circuit and a thermistor glued to the chip. The packaged system is shown in Fig. 4.

Integrating the source in the system could be achieved by setting a small commercial SLED module in the PCB, with an external circulator or coupler to extract the reflected signal. Alternatively, the source could be integrated into the interrogator chip itself, although this solution would require to deal with the potential issues of heat dissipation and stray light.

The photodiodes' electrical outputs were connected to commercial transimpedance amplifiers (model femto-DHPCA-100) with a gain of 10^6 Ω and a bandwidth of 1 MHz. The amplified signals were digitized with two different systems. The passive interrogator signals were acquired with a digital 14-bit oscilloscope model Picoscope 5442D. In the active interrogator scheme, the signals were acquired with an FPGA-based system model RedPitaya Stemlab 125-14, which also generated the modulating sinusoidal signal that was sent to the phase modulators. This system implemented a real-time multitone mixing algorithm and a low pass filter with a frequency cut-off at 700 Hz. The card directly streamed the phase values in digital form to a PC at a sample rate of 1MS/s. Details of the FPGA system implementation are described in [16].

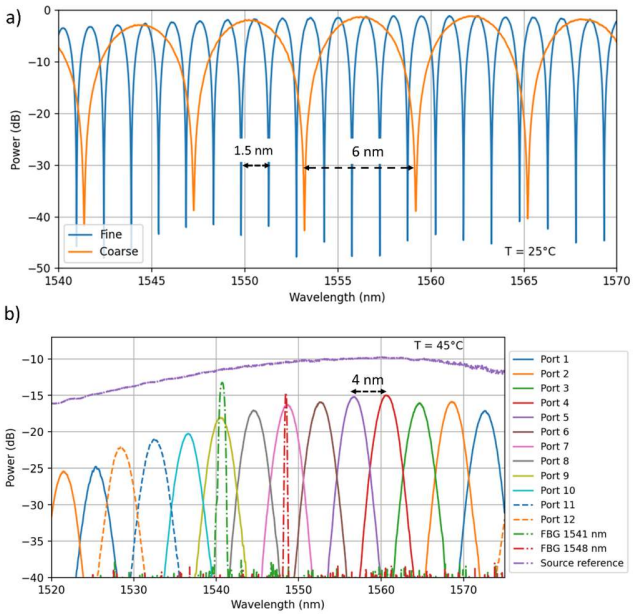

Fig. 3 (a) Spectra of the fine and coarse interferometer, (b) Spectra of the AWG with 12 channels and the 2 FBGs used.

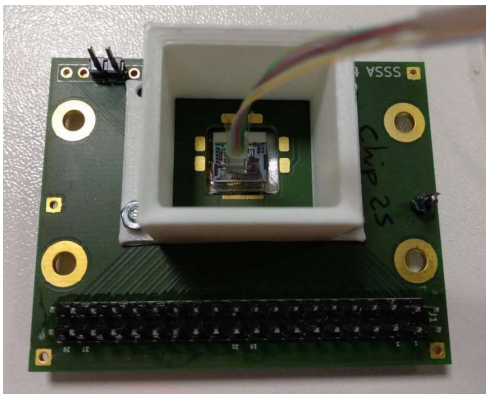

Fig. 4: Packaged chip mounted on PCB with pigtail optical vertical connection and Peltier cell at the bottom.

IV. Experimental Results

This section is divided into 2 parts: multichannel active interrogation with coarse and fine interferometer, and single channel passive interrogation with coarse interferometer. For the active case, the temperature of the chip was set to 45 ºC to match the wavelength of the FBGs with the central wavelength of the corresponding channel of the AWG (see Fig. 3 b)). For the passive interrogation, the temperature was set at 25 ºC as there was no AWG.

A. Active interrogation

Fig. 5 shows the results of the fine interferometer when measuring two sinusoidal signals that excited two FBGs simultaneously (at 80 Hz for the 1548 nm channel and at 130 Hz for the 1540 nm one); these measurements are compared to the ones obtained by the reference interrogator. We found a

very good agreement in the temporal trace signals between our interrogator and the reference one; also, the computed power spectral density (PSD) shows a good agreement for the peaks at the main frequency and the first few harmonics. Note that these harmonics are generated by the PZT actuators, therefore, they are detected in both systems. For the higher-order harmonics, there are some discrepancies that can be attributed to reflected harmonics seen in the reference interrogator since they are close to its Nyquist frequency, and attenuated harmonics in our interrogator as they were close to the cut-off frequency of the low-pass filter. The signal-to-noise ratio (SNR) value for the FBG sensor at 1548 nm was ~80 dB with our interrogator, which is ~5 dB higher than the reference interrogator, whereas, for the 1540 nm FBG, both exhibit ~80 dB of SNR.

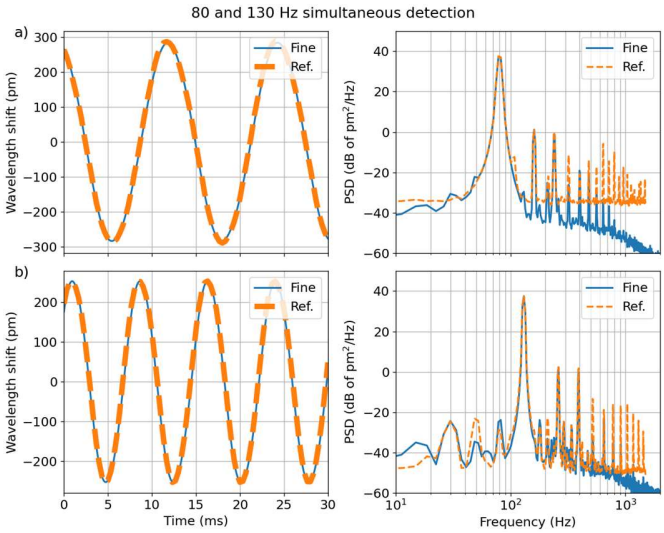

Fig. 5: Measured results using the fine interferometer applying two simultaneous signals at 80Hz on channel at 1548nm (a) and 130Hz at 1540nm (b). On the left we show the temporal signal, and on the right, the PSD of a 5s temporal trace.

The differences between the coarse and fine interferometers can be seen in Fig. 6. In the fine interferometer, a certain wavelength shift in the reflected peak of the FBG would cause a phase shift x4 greater than the coarse one, because of the smaller FSR, as shown in Fig. 3 (a). As a result, the fine interferometer is 4 times more responsive, which can be seen in Fig. 6 a), where the phase signals differ in amplitude by a factor of 4, and the noise floors are similar as shown in the PSD graph. Despite having different responsivities, the wavelength shift $\Delta\lambda$ is the same for both cases, which was calculated using Eq. 2, which takes into account the different responsivities of each interferometer, with $\Delta\phi$ as the input and $\Delta\lambda$ as the unknown variable. Therefore, as seen in Fig. 6 b), the wavelength shifts are the same for both interferometers, but the noise floor of the coarse is ~4 times higher relative to the case of the phase shift. In Fig. 6 c), the noise from the 2 interferometers are compared, where the standard deviation for the fine is σ = 0.13 pm and σ = 0.47 pm for the coarse, which is ~4 times higher than the fine, as expected. As a comparison, the reference has a similar noise floor compared to the fine but has a higher standard deviation σ = 0.28 pm, due to some spurious frequencies.

The dynamic spectral resolutions, defined as the standard deviation over the square root of the bandwidth, are 7.2 fm/Hz$^{1/2}$ for the reference (1.5 kHz bandwidth), 4.9 fm/Hz$^{1/2}$ for the fine (700 Hz bandwidth), and 17.8 fm/Hz$^{1/2}$ for the coarse (700 Hz bandwidth). Although the fine interferometer has a better responsivity, the coarse one has an extended range, as it can retrieve the wavelength within 6 nm (one FSR) unambiguously, while the fine one is limited to 1.5 nm. It is possible to extract the wavelength for signals that exceed one FSR for both the fine and the coarse by phase unwrapping, but this requires continuous tracking of the phase and extra processing.

Finally, Fig. 7 shows the crosstalk from the 1540 nm channel to the 1548 nm channel for the fine interferometer, where we observed a channel isolation of 62 dB. The crosstalk from the 1548 nm to the 1540 nm channel was -56 dB. Crosstalk is most likely due to the limited isolation among the AWG demultiplexer ports.

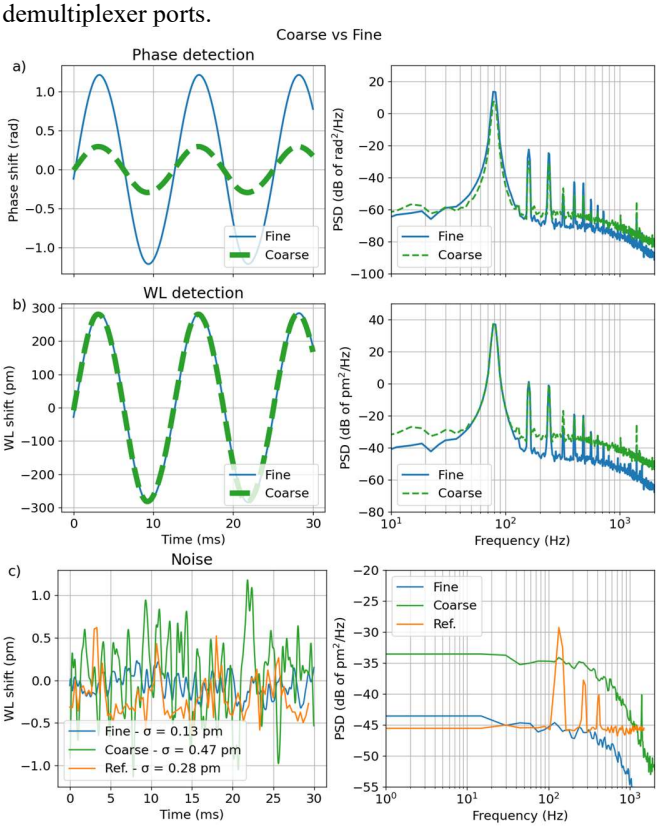

Fig. 6. Comparison between the coarse and the fine interferometer for the FBG at 1548 nm. (a) Applying signal at 80 Hz. (b) Noise measurement also compared with the reference interrogator

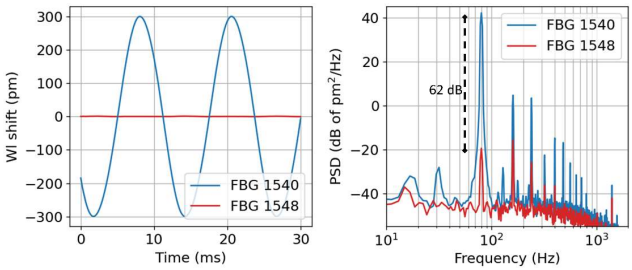

Fig. 7. Crosstalk between two channels of the PIC

B. Passive interrogation

For passive interrogation, the phase modulator (heater) was not used during the measurements. However, it was used for calibration and to test the interferometer. Since the heater response is proportional to the power of its driving signal, if the intended effect is a linear response of the heater, the voltage input signal should be adjusted in such a way that its square is linear. Fig. 8 a) shows the modulation signal sent to the heater in blue, while in red we show its square, which follows a linear curve, while Fig. 8 b) shows the amplified photodiode response of this input signal. The figure also shows fits to sinusoidal signals, which show an excellent agreement, and a phase difference of 93º, which is 3º off from the nominal 90º value. The 3º shift between the 90º-hybrid signals introduces an elliptic distortion in the estimation of the angle, which generates an inaccuracy of the phase measurement of up to 3º in the worst case. This inaccuracy could be corrected by applying a simple correction algorithm similar to the one in [17]. The phase was calculated using the 2 photodiodes signals as inputs in Eq. 4, and then converted to wavelength. Unless otherwise mentioned, a low-pass filter at 10 kHz was introduced for the processing of the data in the PC.

Figure 9 shows the results of the interferometer compared to the reference for different signals applied to the 1548 nm FBG. In Fig. 9 a) the PZT was driven by a sinusoidal signal at 80 Hz; the temporal traces show a very good agreement, and the PSD points out a good match for the main peak and the first few harmonics. However, the PIC version also shows a slightly higher noise floor than the reference interrogator, and a strong peak at 50Hz, which is due to the power line frequency.

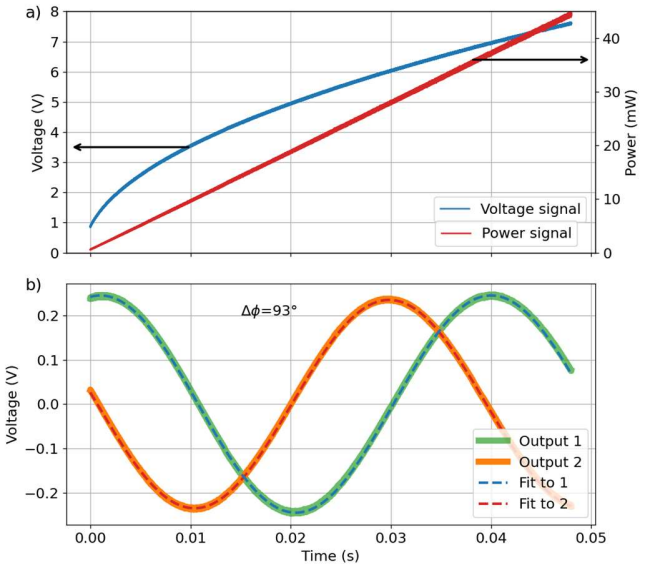

Fig. 8. (a) (Blue) input signal sent to the heater, (Red) Scaled signal of the square of the blue one that represents the intended response of the heater as its response is proportional to the square of the voltage. (b) Photodiodes signal after amplification.

In Fig. 9 b) the FBG was actuated at 1 kHz; note that the signal at the reference interrogator looks under-sampled due to its maximum sampling rate (3 kS/s), while the PIC retrieves the signal with no distortion. In the PSD both interrogators are able to detect the main frequency, but the PIC interrogator can also detect higher harmonics thanks to the extended bandwidth. Finally, in Fig. 9 c), a noise measurement was carried out by applying no signal to the FBG. In this case, it is evident that the PIC noise is dominated by the 50 Hz interference, along with its harmonics and some other spurious frequencies. The standard deviation is σ = 2.55 pm for the PIC interrogator and σ = 0.24 pm for the reference one, although in this case, these numbers are not comparable as the bandwidths are very different. For this case, the dynamic spectral resolutions were not calculated since the noise it is not flat as it is mostly dominated by the 50 Hz interference. For the signal shown in Fig. 9 a), which has a range of variation of 1.2nm, the maximum accuracy error observed using the passive scheme when compared with the reference is +- 25pm, which is the result of the combination of the 50Hz shown in Fig. 9 b) plus the phase error of 3º. The application of the aforementioned ellipse correction algorithm, together with the 50Hz noise reduction through better shielding, would significantly reduce this inaccuracy value.

In order to test the system's frequency limit, we finally applied a sinusoidal signal at 42 kHz, which corresponds to the resonance frequency of the PZT. In this case, the low-pass filter was set at 50 kHz. The response is shown in Fig. 10 (only for the PIC-based interrogator, as this frequency was completely out of the frequency range of the reference interrogator). Although there are several spurious frequencies above 10kHz, the strongest peak is correctly detected at 42 kHz.

Comparing the active and the passive schemes, it is clear that the active demodulation scheme is more tolerant to electromagnetic noise because the demodulation is done far from baseband, while the passive technique is in baseband. In addition, the active scheme only requires one port per measurement point, while the passive technique using the 2x4 coupler needs four optical ports, four photodiodes, and two electrical ports per sensing point (see Fig. 1(a)). This feature complicates WDM multiplexing in the passive scheme, because it would require 4 identical AWGs (one per output port of the 2x4 coupler), and considering a 12-channel AWG, such as the one that was used in the active interrogation, it would require 2x12=24 electrical signals. The main drawback of the active scheme is related to the bandwidth of the phase modulator, which limits our interrogation dynamics to 700Hz, while in the passive scheme the bandwidth is only limited by noise. However, carrier-based phase modulation is also possible in silicon waveguides [18], which would dramatically increase the bandwidth of the active interrogation scheme.

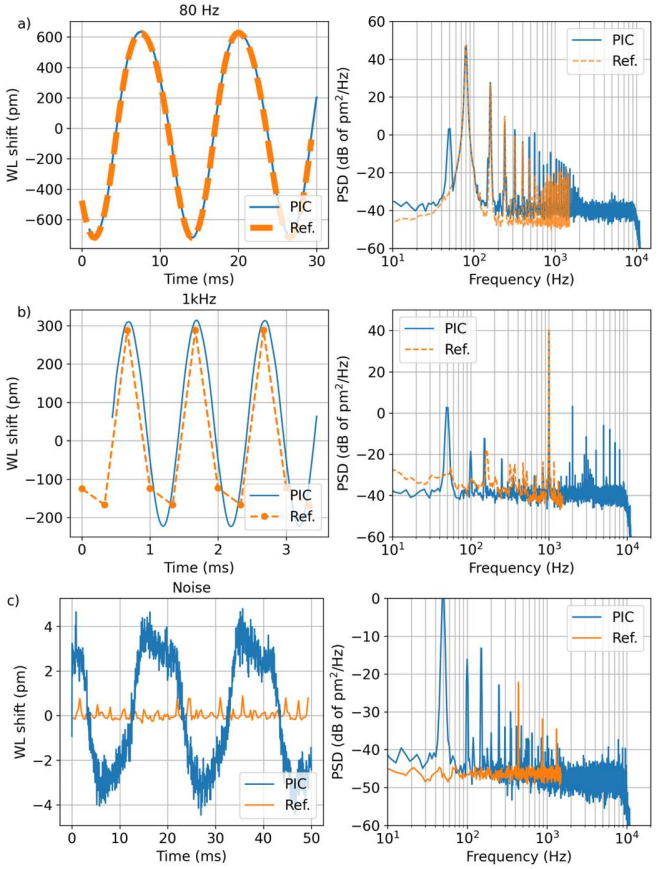

Fig. 9. Comparison of the PIC interrogator with the reference applying different sinusoidal signals to the FBG: a) 80 Hz, b) 1 kHz, c) No signal

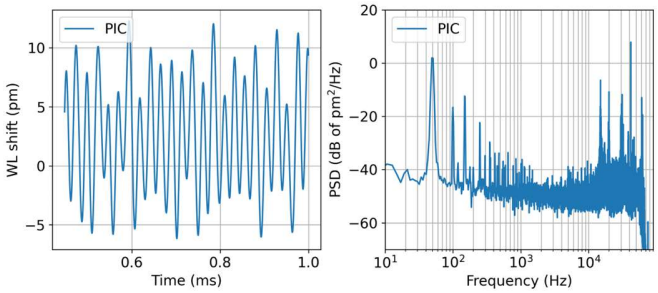

Fig. 10. Signal detection retrieved from the PIC when applying a 42 kHz signal at the FBG.

V. Conclusions

We developed an FBG interrogator based on interferometers built into a miniaturized chip using silicon photonic technology. The active interrogation featured two interferometers, a fine one that features a lower noise level ($\sigma = 0.13$ pm at 700Hz bandwidth, and 4.9 fm/Hz$^{1/2}$ dynamic spectral resolution) with limited range, and a coarse one with an extended range at the expense of higher noise ($\sigma =$ 0.47 pm, and 17.8 fm/Hz$^{1/2}$ dynamic spectral resolution). The passive interrogator featured greater noise but provides a much higher bandwidth, being able to detect signals up to 42 kHz. The same PIC includes different interrogation schemes providing the flexibility to choose the one that is the most suitable for a given application.

References

[1] Siew, S.Y., Li, B., Gao, F., Zheng, H.Y., Zhang, W., Guo, P., Xie, S.W., Song, A., Dong, B., Luo, L.W. and Li, C., "Review of silicon photonics technology and platform development" Journal of Lightwave Technology, 39(13), pp.4374-4389 (2021).

[2] Sahota, J.K., Gupta, N. and Dhawan, D., "Fiber Bragg grating sensors for monitoring of physical parameters: A comprehensive review." Optical Engineering, 59(6), p.060901 (2020).

[3] P. Velha et al., "Monitoring Large Railways Infrastructures Using Hybrid Optical Fibers Sensor Systems," in IEEE Transactions on Intelligent Transportation Systems, vol. 21, no. 12, pp. 5177-5188, (2020).

[4] Guo Honglei et al., "Fiber Optic Sensors for Structural Health Monitoring of Air Platforms", Sensors, (2011).

[5] Dennison, C. R., Wild, P. M., Wilson, D. R., & Gilbart, M. K. An in-fiber Bragg grating sensor for contact force and stress measurements in articular joints. Measurement Science and Technology, (2010).

[6] Trita, A., Voet, E., Vermeiren, J., Delbeke, D., Dumon, P., Pathak, S. and Van Thourhout, D., "Simultaneous interrogation of multiple fiber Bragg grating sensors using an arrayed waveguide grating filter fabricated in SOI platform" IEEE Photonics Journal, 7(6), pp.1-11 (2015).

[7] Tozzetti, L., Bontempi, F., Giacobbe, A., Di Pasquale, F. and Faralli, S., "Fast FBG interrogator on chip based on Silicon on Insulator ring resonator add/drop filters" Journal of Lightwave Technology (2022).

[8] Yang, F., Zhang, W., Zhao, S., Liu, Q., Tao, J. and He, Z., "Miniature interrogator for multiplexed FBG strain sensors based on a thermally tunable microring resonator array" Optics Express, 27(5), pp.6037-6046 (2019).

[9] A. Shen, et al., "Tunable microring based on-chip interrogator for wavelength-modulated optical sensors", Optics Communications, Vol. 340, 116-120 (2015).

[10] Todd, M. D., M. Seaver, and F. Bucholtz. "Improved, operationally-passive interferometric demodulation method using 3× 3 coupler." Electronics Letters 38.15 (2002).

[11] A. Dandridge, A. B. Tveten and T. G. Giallorenzi, "Homodyne Demodulation Scheme for Fiber Optic Sensors Using Phase Generated Carrier," IEEE Journal of Quantum Electronics, vol. 18, p. 1647–1653, (1982).

[12] Y. Marin et al., "Integrated FBG Sensors Interrogation using Active Phase Demodulation on a Silicon Photonic Platform," Journal of Lightwave Technologies, vol. 35, no. 6, pp. 3374-3379 (2017).

[13] Marin, Y.E., Celik, A., Faralli, S., Adelmini, L., Kopp, C., Di Pasquale, F. and Oton, C.J., "Integrated dynamic wavelength division multiplexed fbg sensor interrogator on a silicon photonic chip" Journal of Lightwave Technology, 37(18), pp.4770-4775 (2019).

[14] Marin, Y., Velha, P. and Oton, C.J., "Distortion-corrected phase demodulation using phase-generated carrier with multitone mixing" Optics Express, 28(24), pp.36849-36861 (2020).

[15] https://www.advmf.com/

[16] Elaskar, J., Luda, M.A., Tozzetti, L., Codnia, J. and Oton, C.J., "FPGA-Based High-Speed Optical Fiber Sensor Based on Multitone-Mixing Interferometry" IEEE Transactions on Instrumentation and Measurement, 71, pp.1-11 (2022).

[17] S. H. Chang, H. S. Chung and K. Kim, "Impact of Quadrature Imbalance in Optical Coherent QPSK Receiver," in IEEE Photonics Technology Letters, vol. 21, no. 11, pp. 709-711, June1, 2009, doi: 10.1109/LPT.2009.2016759.

[18] Ruocco, Alfonso, and Wim Bogaerts. "Fully integrated SOI wavelength meter based on phase shift technique." In 2015 IEEE 12th International Conference on Group IV Photonics (GFP), pp. 131-132. IEEE, 2015

Javier Elaskar was born in Córdoba, Argentina in 1994. He received his electronic engineering title in 2018 from Universidad Nacional de Córdoba, Córdoba, Argentina. In 2021 he graduated from a joint masters degree in photonics and networking from Scuola Superiore Sant'Anna, Pisa, Italy, and Aston University, Birmingham, UK. He is currently pursuing a

PhD in emerging digital technologies from Scuola Superiore Sant'Anna, Pisa, Italy, with research topics related with optical fiber sensors and photonic integrated devices.

Philippe Velha was born in France in 1981. He has an msc in integrated electronics and an engineering degree. After his Phd in Physics at three different laboratories: *Institut d'Optique*, *Laboratoire des Technologies de la Micro-electronique* and *SiNaPS* from the *CEA – Grenoble*. In this multi-disciplinary environment he designed, fabricated and measured the first high quality factor integrated micro-cavities known today as nanobeams. He became a research assistant at the University of Glasgow in 2008 where his research field spanned from Silicon Photonics to light modulators, photodetectors and integrated ligh-sources. In 2013, he joined the newly created Silicon Photonics group at *Scuola Superiore Sant'Anna* (Pisa-Italy). In 2022 he was awarded a tenure-track position of assistant professor in Electronics at the University of Trento. His work has been published in several high impact international peer-reviewed scientific journals. He is co-author, of over 100 publications and a book which are regularly cited as reference (over 1000 citations).

Rana M. Armaghan Ayaz was born in Lahore, Pakistan. He received his BSc and MSc in Mechatronics and Control engineering from Universidad of Engineering and Technology , Lahore, Pakistan. He completed his PhD in Biomedical Sciences and Engineering in 2020 from KOÇ University, Istanbul, Turkey with main focus on optical fiber sensors and resonators. He is currently research fellow in Scuola Superiore Sant'Anna, Pisa, Italy, with research focus on interrogation of fiber Bragg gratings, optical fiber sensors and photonic integrated.

Lorenzo Tozzetti was born in Florence, Italy in 1982. He achieved the Bachelor degree in Physics from the University of Florence, Florence, Italy, 2009 and a Master degree in Astrophysics in 2017 from the same university. From 2009 to 2011 worked on the production of Cosmic Dust Analogs in the Department of Physics and Astronomy of the University of Florence, as a research fellow. From 2011 to 2014 worked in the INAF - Astrophysical Observatory of Arcetri, Florence, Italy, as a research fellow, focusing on the characterization of Cosmic Dust Analogs. In the following two years he further developed the same topics at the University of Florence. From 2016 to 2017 worked in the CNR - National Institute of Optics (INO), Florence, Italy, on the development of a prototype for the analysis of the composition of planetary atmospheres. Since 2018 to date has been working in IIM Institute, Scuola Superiore Sant'Anna, Pisa, Italy, as a research fellow, with particular interest on optical fiber sensors and silicon photonic.

Stefano Faralli is assistant professor at Scuola Superiore Sant'Anna. He received the M. Sc. degree in physics from the University of Pisa, Pisa, Italy, in 2000, the M.Sc. degree in optical communications systems and networks from the Politecnico di Milano, Milan, Italy, in 2001, and the Ph.D. degree in telecommunications technology from Scuola Superiore Sant'Anna, Pisa, in 2006. In the period between 2011 and 2012, he was Visiting Scholar at the University of California at Santa Barbara, working in the optoelectronics group. In the period between 2015 and 2017 he was a senior process engineer at the Inphotec center of Scuola Superiore Sant'Anna in charge for the processes of PECVD and LPCVD deposition, wet and dry oxidation. He is co-founder of Infibra Technologies S.r.l., a spin-off company of Scuola Superiore Sant'Anna. He is author and co-author of publications among patens and papers in peer-reviewed international journals and conference digests. His current research interests include optical fiber sensors, integrated optics, silicon photonics, thin film processing, optical amplification for optical communication systems and networks.

Fabrizio Di Pasquale received the degree in electronic engineering from the University of Bologna, Italy, in 1989, and the Ph.D. degree in information technology from the University of Parma, Italy, in 1993. From 1993 to 1998, he was with the Department of Electrical and Electronic Engineering, University College London, U.K., as a Research Fellow, working on optical amplifiers, WDM optical communication systems, and liquid crystal displays. After two years with Pirelli Cavi e Sistemi and two years with Cisco Photonics Italy, he moved to Scuola Superiore Sant'Anna, Pisa, Italy, where he is currently a Full Professor of telecommunications with the Institute of Mechanical Intelligence. He is the Co-founder of Infibra Technologies S.r.l., a spin-off company of Scuola Superiore Sant'Anna, developing and marketing fiber optic sensor systems. He has filed 25 patents and is author or coauthor of more than 250 scientific journals and conference papers. His research interests include optical fiber sensors, silicon photonics, optical amplifiers, WDM transmission systems and networks. He has been the TPC member of several international conferences and on the Board of Reviewers of international refereed journals.

Claudio J. Oton (born in Cartagena, Spain, 1978) received his degree in Physics in 2000 and PhD in 2005 in University of La Laguna (Spain). Then he spent 4 years in the *Optoelectronics Research Centre*, University of Southampton, UK as a post-doctoral researcher and Marie Curie fellow. In 2009 he joined the *Nanophotonics Research Centre*, in Universidad Politecnica de Valencia, (Spain) as a Senior Research Fellow. Finally, in 2012 he joined *Scuola Superiore Sant'Anna* in Pisa (Italy) as an Assistant Professor, and from 2022, Associate Professor. He works in the *Institute of Mechanical Intelligence*, and his main research topic is photonic sensing with integrated photonics and optical fiber technologies. He is author of more than 150 scientific papers and conferences (h-index 26), 3 patents, and has participated in several international research projects and contracts. In particular, he has been coordinator of projects funded by the Italian Space Agency, the Italian Ministry of Economic Development, the EU FP7 program, and has also coordinated several research contracts with industrial partners.